A 3-D model of the influence of meanders on groundwater discharge to a gaining stream in an unconfined sandy aquifer

Nicola Balbarini[1], Wietse M. Boon[2], Ellen Nicolajsen[1], Jan M. Nordbotten[2], Poul L. Bjerg[1] and Philip J. Binning[1]

[1]Department of Environmental Engineering, Technical University of Denmark, Kgs. Lyngby, Denmark, [2] Department of Mathematics, University of Bergen, Bergen, Norway.

Corresponding author: Nicola Balbarini, Department of Environmental Engineering, Technical University of Denmark, Bygningstorvet, Building 115, DK – 2800 Kgs. Lyngby, Denmark, (nbal@env.dtu.dk)

Journal: Journal of Hydrology

Submitted January 2017

Key words: Numerical model, 3-D, Meander, Stream geometry, Spatial and temporal variability, Reach scale.

Abstract

Groundwater discharge to streams depends on several factors, including groundwater flow direction and stream morphology, whose effects are not well understood. Here a 3-D model is employed to investigate the impact of meandering stream geometries on groundwater flow to streams in an unconfined and homogenous sandy aquifer at the reach scale. The effect of meander geometry was examined by considering three scenarios with varying stream sinuosity. The interaction with regional groundwater flow was examined for each scenario by considering three groundwater flow directions. The effect of other parameters on the groundwater flow to a meandering stream was tested for the stream width, the meander amplitude, the magnitude of the hydraulic gradient, and the depth of the aquifer. Implications for a real stream were then investigated by simulating groundwater flow to a stream at a field site located in Grindsted, Denmark. The simulation of multiple scenarios was made possible by the employment of a computationally efficient coordinate transform numerical method. Comparison of the scenarios showed that meanders affect the spatial distribution of groundwater flow to streams. The shallow part of the aquifer discharges to the outward pointing meanders, while deeper groundwater flows beneath the stream and enters from the opposite side. The balance between these two types of flow depends on the aquifer thickness and meander geometry. Regional groundwater flow can combine with the effect of stream meanders and can either enhance or smooth the effect of a meander bend, depending on the regional flow direction. Results from the Grindsted site model showed that real meander geometries had similar effects to those observed for the simpler sinuous streams, and showed that despite large temporal variations in stream discharge, the spatial pattern of flow is almost constant in time for a gaining stream.

Graphical abstract

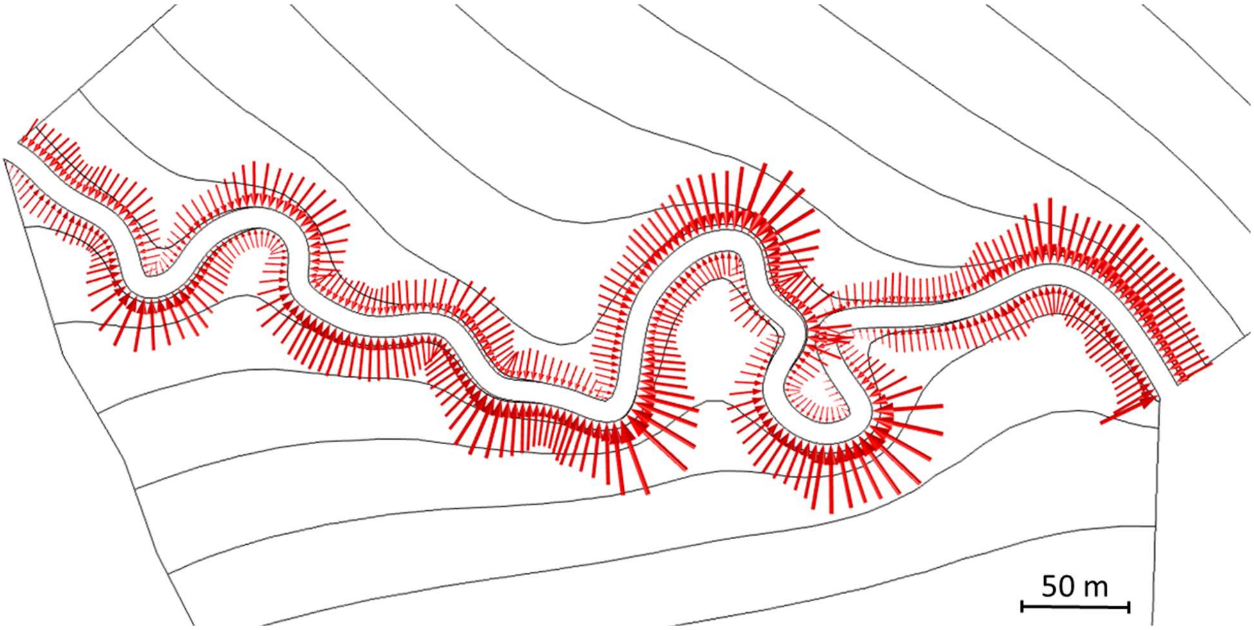

1. Introduction

An understanding of the interaction between groundwater and streams is needed to map water fluxes and the transport of contaminants from groundwater into streams (Cey et al., 1998; Derx et al., 2010; Anibas et al., 2012; Karan et al., 2013; Ou et al., 2013; Freitas et al., 2015). This interaction is governed by several factors such as the hydraulic head difference between the aquifer and the stream, the stream channel geometry, and the hydraulic conductivity distribution of the aquifer and the streambed (Cey et al., 1998; Krause et al., 2007; Anibas et al., 2012; Binley et al., 2013; Fernando, 2013; Flipo et al., 2014). Furthermore, flow processes between groundwater and streams are scale dependent and so must be investigated at different scales (Dahl et al., 2007; Anibas et al., 2012; Flipo et al., 2014; Poulsen et al., 2015).

Investigations of contaminant plume migration to a stream are typically focused on plume scales (10-200 m), which are similar to the stream reach scale (Conant et al., 2004; Byrne et al., 2014; Weatherill et al., 2014; Freitas et al., 2015). At the reach scale, groundwater flow to streams is both vertical and horizontal; thus, an analysis in three-dimensions is required (Harvey and Bencala, 1993; Modica et al., 1998; Flipo et al., 2014). Reach scale groundwater flow paths are not adequately resolved at the larger regional or catchment scales considered by Toth (1963) and many other later larger scale studies (e.g. Wroblicky et al., 1998; Modica et al., 1998; Anibas et al., 2012; Aisopou et al., 2014; Flipo et al., 2014; Gomez-Velez et al., 2015).

Studies investigating reach scale groundwater flow to streams have generally considered straight streams, and have not accounted for the effect of meander bends (Derx et al., 2010; Guay et al., 2013; Miracapillo and Morel-Seytoux, 2014). Thus, a better understanding of how groundwater flow varies in space because of stream meanders is needed (Modica et al., 1998; Diem et al., 2014; Krause et al., 2014; Boano et al., 2014). This is particularly important when investigating contaminant plume discharge to a stream system, where insight is needed to improve site investigations, data interpretation and to design more efficient monitoring campaigns (Harvey and Bencala, 1993; Conant et al., 2004; Anibas et al., 2012; Weatherill et al., 2014).

Only a few studies have analyzed groundwater flow to meandering streams (e.g. Dahl et al. (2007), Nalbantis et al. (2011), Flipo et al. (2014), and Boano et al. (2014)). A literature review is shown in Table S1 and shows that the majority of research on meandering stream-aquifer interaction has focused on the hyporheic processes (Wroblicky et al., 1998; Salehin et al., 2004; Cardenas et al., 2004; Cardenas 2008; Revelli et al., 2008; Cardenas, 2009a; Cardenas, 2009b; Boano et al., 2006; Stonedahl et al., 2010; Boano et al., 2009; Boano et al., 2010, Brookfield and Sudicky, 2013; Gomez-Velez et al., 2014; Gomez-Velez et al., 2015). Hyporheic processes take place in the hyporheic zone just under the stream bed, where stream water mixes with groundwater, before returning to the stream. For example, Boano et al. (2010) applied an analytical approach to examine 3-D groundwater flows directly under a streambed, but did not consider the surrounding groundwater flow system.

For many problems, it is necessary to move beyond the hyporheic zone, and consider larger scale groundwater flows at the reach scale. Thus, the focus of this paper is groundwater flow to meandering streams at the reach scale. The model of Cardenas (2009a; 2009b) is particularly relevant for this paper. It presents a 2-D model with focus on the hyporheic exchange within stream meanders. Here that model is extended to 3-D and the analysis focuses on the groundwater flow to the stream. It is important to examine groundwater flow to streams in three dimensions because these systems typically have very strong vertical flow components which cannot be captured in two-dimensional models. The extension to three dimensions will be shown to lead to new insights on the patterns of groundwater flow. These insights are particularly important in studies of contaminant discharge to streams because it is critical to be able to link measured contaminant discharges at the stream with contaminated sites located further away from the stream.

This study analyses the spatial variability of the groundwater flow discharge to streams along meander bends in a full 3-D system at the reach scale. The first aim is to simulate the groundwater flow paths to streams and investigate how those paths are affected by stream meanders and groundwater flow direction in the aquifer. A 3-D model is presented simulating the discharge to streams for a synthetic gaining sinuous stream with three scenarios of sinuosity: a straight stream, a moderately sinuous stream, and a highly sinuous stream. For each scenario, three groundwater flow directions are assumed with the dominant groundwater flow being: perpendicular to the stream; along the stream; and diagonally across the stream. In addition to the stream sinuosity and the groundwater flow direction, the effects of other parameters on the groundwater flow to a sinuous stream were tested: the stream width, the meander geometry, the aquifer thickness, and the magnitude of the hydraulic gradient. The second aim is to apply the 3-D model to a meandering stream at Grindsted in Denmark in order to assess the effects in a field scale system with a real geometry and time varying stream water levels. Finally the implications for our current understanding of discharges to streams are discussed.

To address these aims, the 3-D numerical model was developed using a novel coordinate transformation method developed by Boon et al. (2016). This method solves the equation for groundwater flow in a transformed domain, which is constant in time, while the coordinate system changes depending on the groundwater free surface variations. The application of the linear transformation allows the transformed domain geometry to be simpler than the original problem; thus, the method is computationally efficient and can be applied to complex geometries. Boon et al. (2016) employs the method to simulate groundwater flow to wells, but it has not been applied to other relevant groundwater systems. Since the application of the coordinate transform method to groundwater/surface water interaction is new, it was first tested and compared to existing approaches (the moving mesh and the saturated-unsaturated groundwater flow method). It is shown that the coordinate transform method is far more computationally efficient than the other methods. This was important for this study since it involved the analysis of many scenarios and so an efficient method is needed.

2. Method

2.1 **Sinusoidal stream model**

In this study, the effect of the stream sinuosity on the groundwater flow to streams is analyzed by extending the two-dimensional steady state model developed by Cardenas (2009a; 2009b) to three dimensions. The stream is assumed to be sinusoidal with a constant wavelength (λ) of 40 m and amplitude (α), which is varied in order to reproduce different levels of sinuosity. The sinuosity (S) is calculated by dividing the sinuous stream length along the channel by the straight valley length (300 m in this study). Three sinuosity scenarios (Figure 1) are considered: a) straight stream (S=1, α=0 m), b) moderately sinuous stream (S=1.14, α=5 m), and c) a highly sinuous stream (S=1.74, α=13.5 m). The choices of sinuosity, wavelength, and amplitude are the same as those of Cardenas (2009a; 2009b).

The spatial variability of the groundwater flow to the stream is affected by the stream morphology, the groundwater flow direction, and the distribution of hydraulic conductivities (Krause et al, 2012; Gomez-Velez et al., 2014). In order to isolate and analyze the effect of the stream morphology and the groundwater flow direction, the aquifer is assumed to be homogenous and isotropic with a hydraulic conductivity of 40 m/d. The stream cross section is a half-ellipsoidal with a depth of 3 m and a width of 5 m. The stream-aquifer interface is a constant-head boundary where the head varies linearly along the channel with a gradient determined by dividing the overall gradient in the x direction (0.001) by the sinuosity. Thus, the stream is a gaining stream along the entire length. The top and bottom boundary, except for the stream boundary, are no-flow boundaries and the remaining boundaries are constant-head boundaries. The head gradient is assumed to change linearly depending on the direction.

In order to simulate different groundwater flow directions, the head gradient on the boundary in the x-direction and in the z-direction are constant (0.001 and 0 respectively) while the y-direction gradient is 0.004 for simulating regional groundwater directed laterally toward the stream and 0.0005 for regional groundwater flowing in the direction of stream flow. These values were selected based on Cardenas (2009a, 2009b). The third groundwater flow scenario assumes groundwater directed south-west diagonally across the stream, with a boundary gradient in the y-direction of 0.0005 in the area north of the stream and 0.0001 south of the stream.

The effect of the gradient on the x-direction was tested by simulating a low gradient of 0.001, also used for the other simulations, and a high gradient of 0.01. The assumption of a constant aquifer thickness of 40 m was tested by modeling a shallower aquifer with a thickness of 5 m and a deeper aquifer with a thickness of 80 m. Similarly, different stream morphology were tested by varying the stream width between 2 and 10 m, and the meander wavelength between 20 and 80 m. These scenarios were simulated for the highly sinuous stream and groundwater flow directed laterally toward the stream.

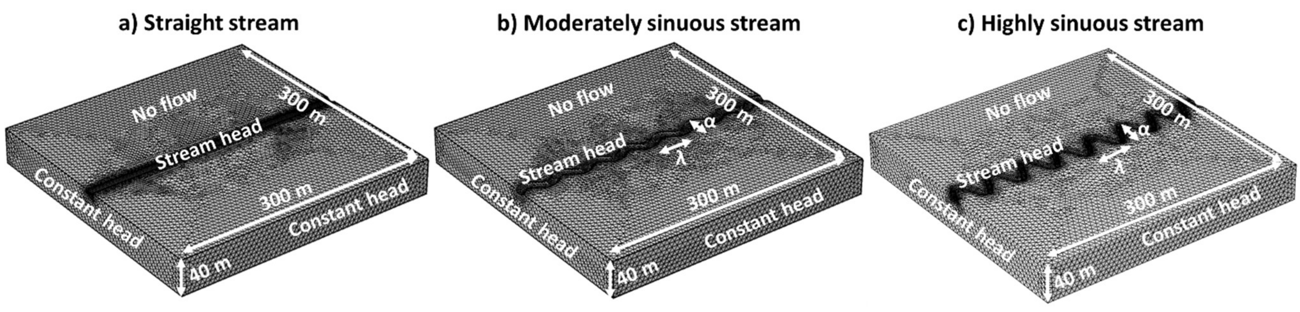

Figure 1: Model domain, finite element mesh, and boundary conditions for the three scenarios of the synthetic stream model: straight stream (a), the moderately sinuous stream (b), and the highly sinuous stream (c) models.

2.2 **Grindsted stream field site**

To examine the implications of findings for real streams with more complex geometries with time varying boundary conditions, a 500 m reach scale model of a field site in southern Jutland, Denmark (Figure 2) was constructed. Grindsted stream has a catchment area of approximately 200 km^2, is 1-2.5 m deep and 8-12 m wide. The unconfined aquifer is 80 m thick and is in hydraulic contact with the stream. The geology is composed of a Quaternary sandy formation for the first 10-15 mbgs and, below that, a Tertiary sandy formation. The aquifer is underlain by a thick and extensive Tertiary clay layer at 80 mbgs (Barlebo et al., 1998; Heron et al., 1998). Two contaminated sites are present in the surrounding area: Grindsted factory located 1.5 km north of the stream, and Grindsted landfill located 2 km south of the stream (Kjeldsen et al., 1998). From these sites, contaminant plumes discharge into the stream, as evident by examination of stream water quality made by Nielsen et al. (2014) and Rasmussen et al. (2015). The model domain was constructed in order to include the area where the contaminant plumes discharge to the stream. This paper focuses on a detailed mapping of groundwater flows adjacent to the stream. The analysis of the coupled contaminant transport processes is beyond the scope of this paper and will not be discussed further.

The regional equipotential map (Figure 2) was used to define the lateral extent of the model domain and its geometry. Equipotential boundaries, where the flow is perpendicular to the boundary and the head is constant over depth, are employed (Aisopou et al., 2015). The remaining boundaries are placed along streamlines where a no-flow condition is assumed on vertical sides. The temporal variability of groundwater flow to streams was modelled accounting for variation in precipitation, stream water level and groundwater head. Precipitation data were collected by the Danish Meteorological Institute at a measurement station at Billund Airport, 15 km from the study site (DMI, 2015). The temporal variation in groundwater heads was monitored at several wells in the

Grindsted area (selected wells are shown in Figure 2). Well 114.1996 was used to set the variable head on the southern boundary, adjusting all measured heads by 1.2 m because the well is not located exactly on the boundary. Similarly, well 114.1447 was applied on the northern boundary, assuming a head difference of 0.9 m. The adjustment was made as part of the model calibration in order to fit the simulated with the observed groundwater head level at the two wells located inside the model domain: 114.1448 and 114.1997. During the model calibration, values of 30 m/d for the horizontal hydraulic conductivity and 3 m/d for the vertical hydraulic conductivity were selected. These values are being similar to the hydraulic conductivities from other field and model studies in the area (Barlebo et al. 1998; Bjerg et al., 1995; Lønborg et al., 2006).

Stream water level data was obtained at the Tingvejen gaging station, located 2.5 km upstream of the model domain, and at Eg Bro, located 8.1 km downstream of the model domain. The average water slope between the two gaging stations is 0.001. The mean annual stream discharge is 2,150 l/s at Tingvejen and 2,980 l/s at Eg Bro. The simulated stream reach is about 900 m long and the annual average groundwater discharge to the stream in the reach, estimated from annual average discharge measurements from the gaging stations, is 70 l/s.

The model assumes 80 m deep homogenous sandy aquifer with a hydraulic conductivity of 30 m/d in the horizontal direction and 3 m/d in the vertical direction. The stream cross section is half-ellipsoidal with depth of 3 m and width of 10 m. The depth of 3 m is larger than the stream water depth to allow for in stream head variations without overbank flow. The stream is implemented as a time varying head boundary where the head varies linearly along the channel with a gradient of 0.001, corresponding to the average water slope between the two gaging stations. The slope of the streambed is assumed to be 0.001, as to the stream water slope.

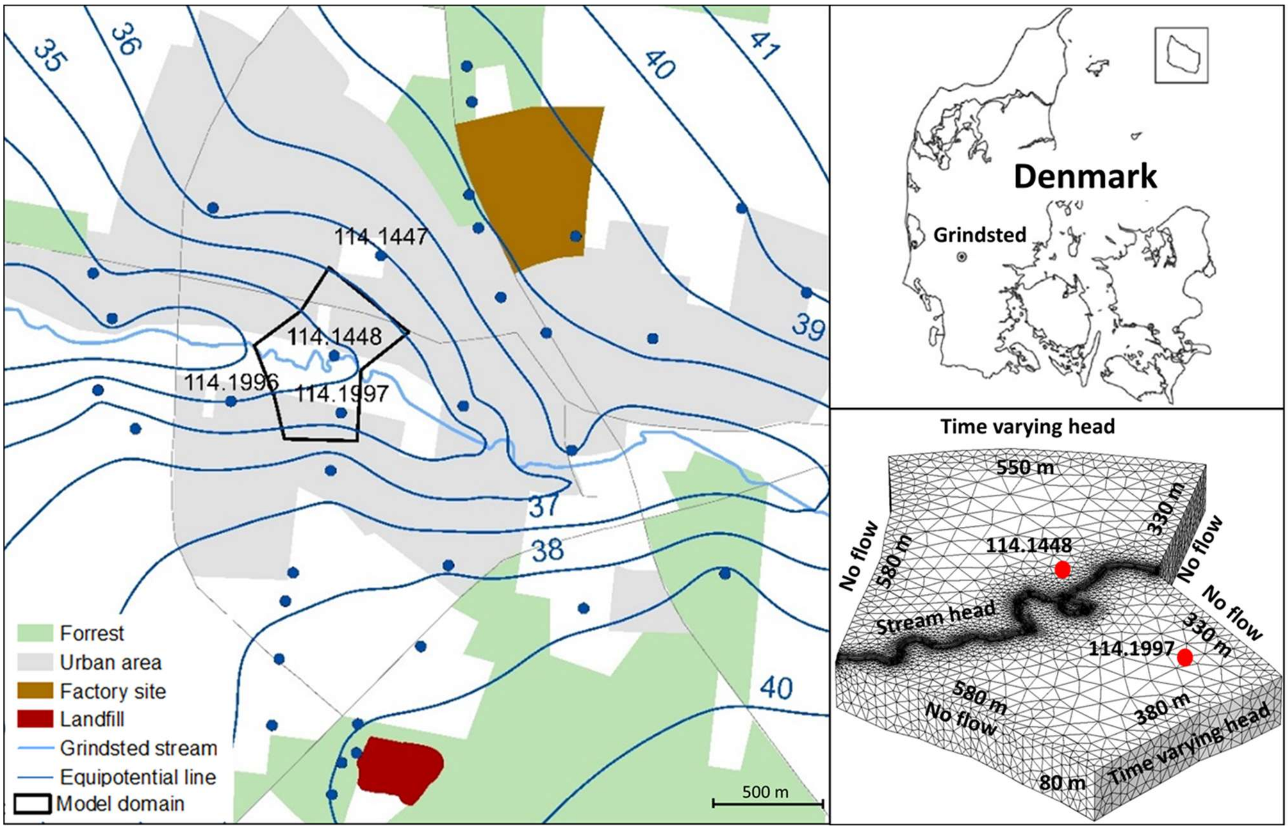

Figure 2: Overview of the Grindsted stream study site and model set up. The blue lines indicate the equipotential lines with an interval of 1 m. The equipotential map is based on groundwater head measurements collected at the wells indicated by the blue dots. The name of the observation wells used to set up boundary conditions or for comparison with model results are shown on the map. The model domain area is defined by the black line. The close up on the bottom right shows the model grid, the boundary conditions, the model size, and the location of boreholes located inside the model domain.

2.3 Modelling groundwater flow to streams with the coordinate transformation method

The groundwater head variability which controls the flow to/from the stream is difficult to resolve with a traditional groundwater flow model employing a regular grid. Several methods have been developed to describe the variability of groundwater head in unconfined aquifers: the moving mesh (Knupp, 1996; Darbandi et al., 2007; Bresciani et al., 2011) and the saturated-unsaturated groundwater flow (Freeze, 1971; Dogan and Motz, 2005; Keating and Zyvoloski, 2009; Camporese et al., 2010). An overview of studies applying these methods is provided in Table S2. These methods were developed for unconfined aquifers without considering stream interaction, which introduces large local variations in groundwater head.

The moving mesh method solves the groundwater flow problem under saturated conditions and adjusts the mesh depending on the groundwater head calculated at the previous time step. The method requires re-meshing at each time step, which is very computationally demanding (Freeze, 1971; Kinouchi et al., 1991; Knupp 1996) and can fail for large changes in the water head between two time steps or for steep gradients, such as at the stream aquifer interaction (Bresciani et al., 2011; COMSOL, 2013). The saturated-unsaturated method solves the flow equation under both saturated and unsaturated conditions avoiding the problem of explicitly describing the water table surface (An et al. (2010) and Kinouchi et al. (1991)). However, the method is computational demanding and is rarely justified when the main focus is the saturated flow (Keating and Zyvoloski, 2009).

The new coordinate transformation of Boon et al. (2016) was used to solve the groundwater flow equations in the model domain. The method reduces computational time by employing a coordinate transformation so that the saturated groundwater flow equations are solved on a fixed mesh (Figure 3). For comparison purposes, the equations were also solved on a domain with a dynamically deforming mesh, and by a coupled saturated/unsaturated flow solver (Supportive information S1).

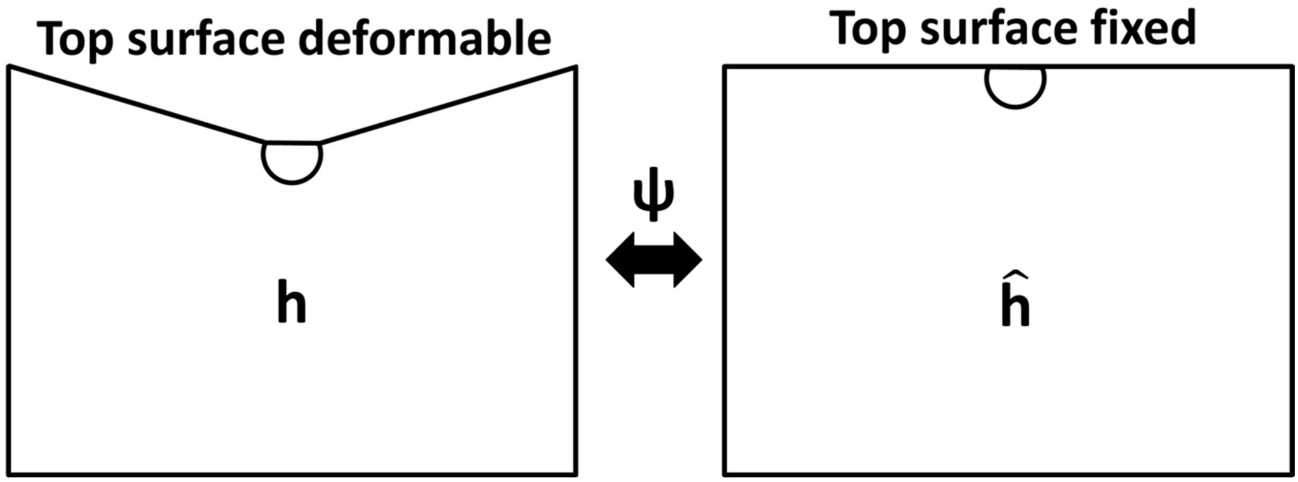

Figure 3: The coordinate transformation method for modelling unconditioned aquifers interacting with streams of Boon et al. (2016) employs a fixed domain (right) instead of the real deformable domain (left). A coordinate transformation Ψ is used to map the governing equations between the two domains.

To test the three methods for the groundwater flow to streams problem, they were implemented for a two-dimensional study case and their computational accuracy and efficiency compared (Section S1 in the supportive information). The comparison between the methods is shown in the supporting information (Table S4), where it can be seen that the coordinate transformation method is the least computational demanding of the three methods for a 2-D test problem, requiring 32 times less computational effort than the saturated-unsaturated approach and 3 times less time than moving mesh, for a relatively coarse discretization. Differences become larger in 3-D and when the grid is refined: the computational time required by the moving mesh in a 3-D test (137 min) is 32 times more computational time than the coordinate transformation (4 min). Furthermore, the coordinate transformation method does not lead to instabilities and oscillations, problems that were encountered with the moving mesh. The coordinate transformation is a much more computationally efficient solution making it possible to simulate a variety of scenarios and properly explore the problem. Thus, the coordinate transformation method is employed for all examples in this study.

In the coordinate transformation method (Boon et al., 2016), the groundwater flow equation for saturated conditions is solved in a transformed domain $\widehat{\Omega}$:

$$S_s \frac{\partial \hat{h}}{\partial t} + \nabla \cdot \left(- \widehat{\mathbf{K}} \cdot \nabla \hat{h}\right) = 0 \qquad \text{in } \widehat{\Omega} \qquad (1)$$

Where Ss is the specific yield [1/m], $\hat{h}$ is the hydraulic head in the transformed space [m] and $\widehat{K}$ is the hydraulic conductivity tensor in the transformed space [m/s]. The groundwater flow velocity in the transformed domain $\widehat{\Omega}$ becomes:

$$\hat{q} = -\widehat{\mathbf{K}} \cdot \nabla \hat{h} \qquad (2)$$

The conditions at the top boundary Γ are:

$$\hat{h}(\hat{x}, t) = \zeta(\hat{x}, t) \qquad \text{on } \Gamma \qquad (3)$$

$$-\mathbf{e}_{\Gamma} \cdot \left(-\widehat{\mathbf{K}} \cdot \nabla \hat{h}\right) = \left(I - S_y \frac{\partial \zeta}{\partial t}\right) \qquad \text{on } \Gamma \qquad (4)$$

where S_y is the specific yield [-],ζ is the elevation for the free surface [-], and e_Γ is the unit normal to Γ. The governing equations are solved in Comsol Multiphysics, which employs a finite element numerical approximation (COMSOL, 2013). The finite element method employs the weak form of (1) with a linear polynomial Lagrange test function $g \in H^1(\widehat{\Omega})$ which is combined with the boundary equation (4) and input into COMSOL Multiphysics:

$$\left(S_s \frac{\partial \hat{h}}{\partial t} + \nabla \cdot \left(- \widehat{\mathbf{K}} \cdot \nabla \hat{h}\right), g\right)_{\widehat{\Omega}}$$

$$= \left(S_s \frac{\partial \hat{h}}{\partial t}, g\right)_{\widehat{\Omega}} + \left(\widehat{\mathbf{K}} \cdot \nabla \hat{h}, \nabla g\right)_{\widehat{\Omega}} + \left(\mathbf{e} \cdot \left(-\widehat{\mathbf{K}} \cdot \nabla \hat{h}\right), g\right)_{\Gamma}$$

$$= \left(S_s \frac{\partial \hat{h}}{\partial t}, g\right)_{\widehat{\Omega}} + \left(\widehat{\mathbf{K}} \cdot \nabla \hat{h}, \nabla g\right)_{\widehat{\Omega}} - \left(\left(I - S_y \frac{\partial \zeta}{\partial t}\right) e_{\Gamma_z}, g\right)_{\Gamma} = 0 \qquad (5)$$

The linear transformation ψ is:

$$\mathbf{x} = \psi(\hat{x}, \hat{z}, t) = [\hat{x}, 0] + \zeta(\hat{x}, t)\hat{z}\mathbf{e}_{\mathbf{z}} \qquad (6)$$

$$h(x,z,t) = \hat{h}(\hat{x},\hat{z},t) \quad (7)$$

where e_z is the unit vector in the z-direction. The hydraulic conductivity field is a function of the elevation of the free surface ζ and can be derived from the linear transformation:

$$\begin{aligned}\widehat{\mathbf{K}}(\hat{x},\hat{z},t) &= \det \widehat{\nabla}\psi \, (\widehat{\nabla}\psi)^{-1}\mathbf{K}(\widehat{\nabla}^{T}\psi)^{-1} \\ &= \zeta\begin{bmatrix} K_h & -K_h\hat{z}\zeta^{-1}\widehat{\nabla}\zeta \\ -K_h\hat{z}\zeta^{-1}\widehat{\nabla}^{T}\zeta & \left(K_h\hat{z}^{2}\widehat{\nabla}^{T}\zeta\widehat{\nabla}\zeta + K_v\right)\zeta^{-2}\end{bmatrix}\end{aligned} \quad (8)$$

In equation (8) $\zeta = \zeta(\hat{x},t)$, $K_h = K_h(x,z)$, $K_v = K_v(x,z)$, and $\widehat{K}$ depends on the linear transformation described in equation (6) and (7).

Apart from the boundary condition for the top boundary (5), the boundary conditions applied in the transformed domain are: no-flow for the bottom boundary, and time-variable fixed-head for the lateral boundaries. The transform formulation, as well as its numerical implementation using lowest-order Lagrange finite elements is provably stable and convergent (Boon et al., 2016).

3. Results

3.1 Horizontal variability of the groundwater flow to the stream

The groundwater discharge to the stream at the upper edge of the stream-aquifer interface is shown in Figure 4, where the red arrows are proportional to the horizontal groundwater discharge. Table 1 shows the total flux to a meander from both stream sides (m/s) for each scenario and the percentage of flow discharged at the outward pointing side of the meander and at the inward pointing side of the meander.

The straight stream has a constant discharge along the stream for all hydraulic gradients (Figure 4a, 4b, and 4c), except for at the boundaries, where the boundary conditions have affected the results. In the moderately sinuous stream (Figure 4d, 4e, and 4f), the groundwater discharge to the stream is not constant and changes depending on the location along the stream meander, as shown by the arrow size. The discharge is largest at the extremes of the stream meanders, with 62% and 60% of the groundwater flux entering the stream on the outward pointing side of the meanders for a J_{yx} of 4 and 0.5 respectively (Table 1). This variation in the groundwater discharge to the stream is due to the stream sinuosity and increases with the sinuosity: 73% and 75% of the groundwater flux enters at the outward pointing side of the meander for a J_{yx} of 4 and 0.5 respectively. This effect can also be seen by comparing Figure 4d and 4f with Figure 4g, 4h.

The ratio between the hydraulic gradient in the y and x-direction (J_{yx}) affects the groundwater direction to the stream. In the straight stream, for a large J_{yx} (Figure 4a), the groundwater direction is more perpendicular to the stream compared to a lower J_{yx} (Figure 4b). When two different values of J_{yx} are applied on each side of the stream (Figure 4c), both the direction of the groundwater to the stream and the magnitude of the discharge change as the stream is crossed: the lower value of J_{yx} in the southern side corresponds to a lower groundwater discharge to the stream. Therefore, the percentage of groundwater flux to the stream is higher on the northern side (69%), where the hydraulic gradient in the y-direction is higher, compared to the southern side (31%).

The effect of the hydraulic gradient, described for the straight stream, can also be observed in the moderately (Figure 4f) and highly sinuous stream (Figure 4i), combined with the effect of the sinuosity. The highest groundwater flow to the stream is located further upstream on the outward pointing side of the meander bend when decreasing the value of J_{yx}. Therefore, the groundwater flux on the outward pointing side increases from 60% to 67% for the moderately sinuous stream, when the flux is measured on the meander pointing north, where the gradient in the y-direction is higher. The effect of the gradient decreases when the sinuosity increases: for the highly sinuous stream the flux increases to 75% to 76%.

Table 1: Total groundwater fluxes to the stream at a meander and percentage of the fluxes entering the stream on the outward pointing side and on the inward pointing side of the meander. The total flux was calculated as the integral of the discharge along the meander at the stream-aquifer interface divided by the interface area.

Model	Sinuosity	Meander side	J_{yx} = 4	J_{yx} = 0.5	J_{yx}^{north} = 0.5 J_{yx}^{south} = 0.1
Straight stream	1	Northern side [%]	50	50	69
		Shouthern side [%]	50	50	31
		Total [m/s]	1.02	0.104	0.073
Moderately sinuos stream	1.14	Outward side [%]	62	60	67
		Inward side [%]	38	40	33
		Total [m/s]	1.01	0.116	0.092
Highly sinuous stream	1.74	Outward side [%]	73	75	76
		Inward side [%]	27	25	24
		Total [m/s]	0.73	0.088	0.087

The results shown in Figure 4 and Table 1 are based on simulations where all parameters are assumed to be constant, except for the amplitude of a meander, and consequently the stream sinuosity, and the ratio between the hydraulic gradient in the y and x-direction. The parameters that were not varied include the wavelength of a meander (40 m), the hydraulic gradient in the x-direction (1‰), the stream width (5 m), and the aquifer depth (40 m). In order to study the effect of these assumptions, additional simulations were performed for the scenario with highly sinuous stream and J_{yx} of 4. The effect of these parameters on the groundwater discharge to the stream is summarized in Table 2, where the bulk values indicate the parameter value used for the simulations in Table 1 and Figure 4. The figures showing the horizontal groundwater flow to the stream for the scenarios summarized in Table 2 are provided in the Supporting Information.

The groundwater flux to a stream meander increases with the hydraulic gradient in the x-direction, from 0.73 m/s to 7.04 m/s for a hydraulic gradient of 1‰ and 10‰ respectively. The groundwater flux decreases when increasing the stream width, from 1.15 m/s to 0.52 m/s for a 2 m and a 10 m wide stream. However, the percentages of groundwater entering the stream on one side or the other of the meander do not change. This indicates that the magnitude of the hydraulic gradient and the stream width do affect the magnitude of groundwater flow entering the stream, but not the direction of the groundwater flow to the stream.

The wavelength of the stream sinuosity does not affect the total discharge to the stream, but affects the percentage of groundwater entering on each side of a meander bend. The groundwater flux on the outward pointing side of a meander decreases, from 78% to 64%, by increasing the wavelength, from 30 to 80 m. When keeping constant the amplitude of a meander and increasing the wavelength, the sinuosity of the stream decreases. Thus, the percentage of water entering the outward pointing side of the meander decreases with the sinuosity. This confirms the observation made for the moderately sinuous stream and the highly sinuous stream in Table 1. Furthermore, this result highlights that the groundwater flow to the stream depends on the sinuosity, and not the amplitude or the wavelength of the meanders.

The groundwater flux decreases when increasing the aquifer depth. This effect is small for the low and the middle value tested: from 0.72 m/s to 0.73 m/s for an aquifer depth of 5 m and 40 m, respectively. When testing an 80 m deep aquifer, the groundwater flux to the stream increases up to 1.90 m/s. The percentage of water entering the stream on the outward pointing side of a meander is also affected and decreases from 75% for the 5 m deep aquifer to 69% for the 80 m deep aquifer.

Based on the analysis of the horizontal groundwater flow to the stream and the groundwater fluxes to a meander, the parameters affecting the spatial distribution of the groundwater flow to a stream are the groundwater flow direction, the stream sinuosity, and the aquifer depth. Therefore, the effect of these parameters is further analyzed by looking at the groundwater flow to the stream in a vertical cross section, in Section 3.2.

Table 2: Groundwater discharge to the stream at a meander stream. Only one parameter at the time has been changes, the other are the same as the simulations described in the method. The bulk values are the ones used for the simulations describe in Table 1 and in Figure 4-6. Two parameters have not been changed, since their effect has already been analyzed in Table 1: ratio between the hydraulic gradient in the y- and x-direction (J_{yx} = 4) and the meander amplitude (α = 13.5)

Meander side	**Wavelength [m]**			**Hydraulic gradient in the x-direction [‰]**		**Stream width [m]**			**Aquifer depth [m]**		
	30	**40**	80	**1**	10	2	**5**	10	5	**40**	80
Outward side [%]	78	**73**	64	**73**	72	72	**73**	75	75	**73**	69
Inward side [%]	22	**27**	36	**27**	28	28	**27**	25	25	**27**	31
Total [m/s]	0.51	**0.73**	0.72	**0.73**	7.04	1.15	**0.73**	0.52	0.72	**0.73**	1.90

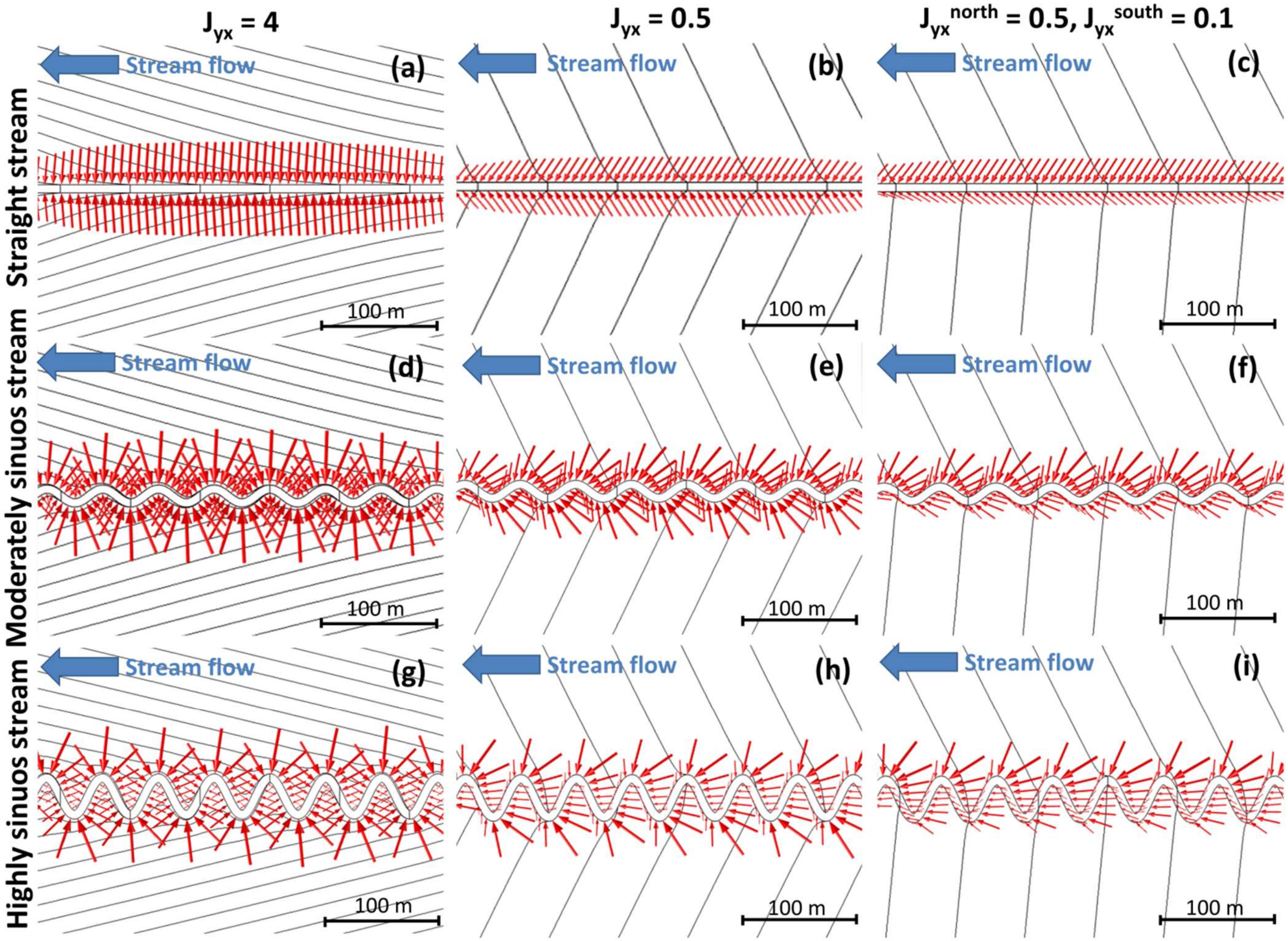

Figure 4: Groundwater discharge to the stream at the upper edge of the stream-aquifer interface shown by the red arrows, which are proportionate to the flow. The equipotential lines separated by a 0.05 m interval are indicated by the black lines. Jyx represent the ration between the hydraulic gradient in the y and in x-direction. The moderately sinuous stream has sinuosity (S) of 1.14 and amplitude (α) of 5 m. The highly sinuous stream has sinuosity (S) of 1.74 and amplitude (α) of 13.5 m.

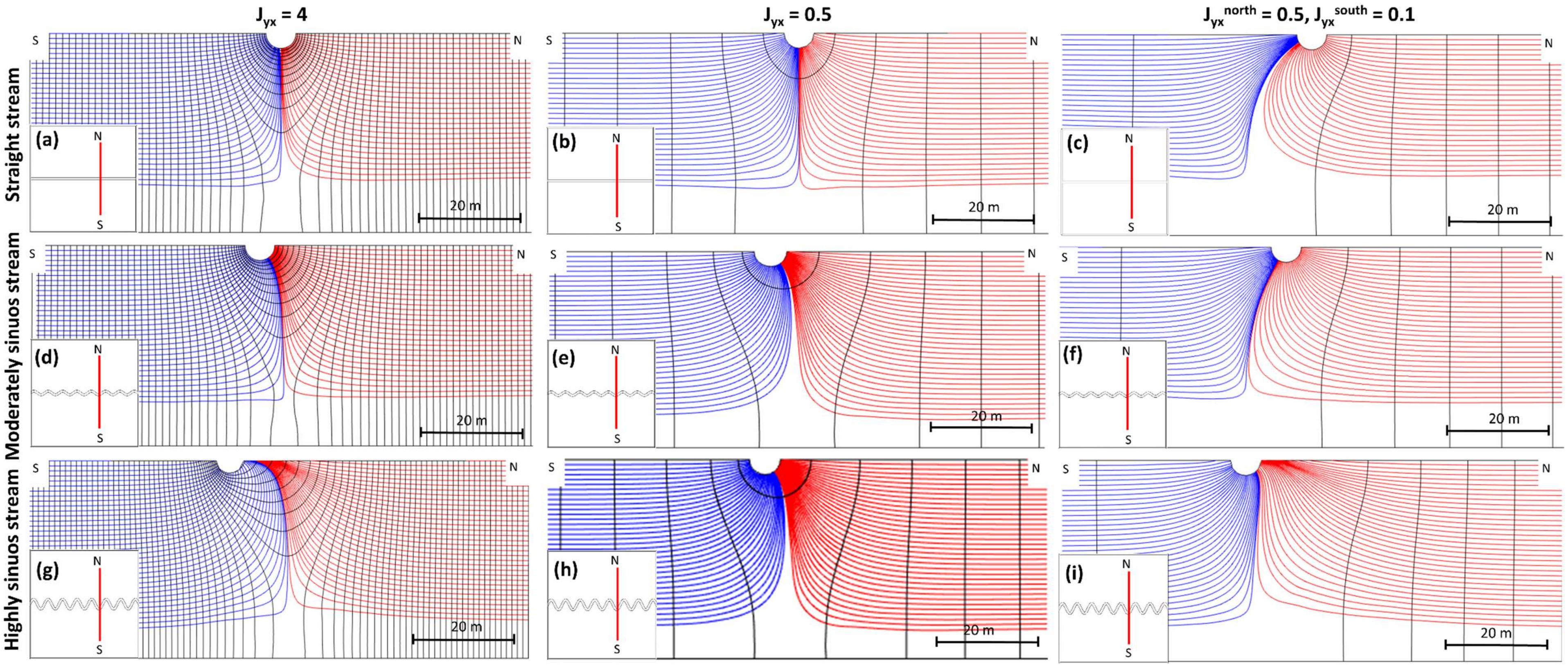

Figure 5: Groundwater paths from the northern side of the stream (red lines) and from the southern side of the stream (blue lines) at a vertical cross section perpendicular the stream and located at the edge of a meander pointing south. The black lines show the equipotential lines separated by 0.005 m interval. Jyx represent the ration between the hydraulic gradient in the y and in x-direction. The moderately sinuous stream has sinuosity (S) of 1.14 and amplitude (α) of 5 m. The highly sinuous stream has sinuosity (S) of 1.74 and amplitude (α) of 13.5 m.

3.2 **Vertical variability of the groundwater flow to the stream**

In order to analyze the vertical spatial variability of the groundwater close to the stream, the groundwater flow direction on a vertical cross section perpendicular to the stream is shown in Figure 5 with particle tracks to highlight the streamlines: blue for the particles originating south of the stream and red for particles originating from the north. The contour lines (black lines) show the groundwater head with a distance of 0.005 m.

In the straight stream (Figure 5a and 5b), the groundwater streamlines enter the stream on the side from which it originates when J_{yx} is constant on model boundaries. In Figure 5c, the hydraulic gradient in the y-direction is larger on the northern side of the stream compared to the southern side. Here, the groundwater streamlines coming from the north enter the stream both on the northern and southern side of the stream, with the discharging bank depending on the depth of origin of the groundwater flow.

In the moderately sinuous stream and in the highly sinuous stream, the cross section was placed at a point with a meander pointing south. When the hydraulic gradient in the y-direction is the same on both sides of the stream (moderately sinuous stream: Figure 5d and 5e; highly sinuous stream: Figure 5g and 5h), the groundwater streamlines coming from the south enter the stream both on the southern and northern side of the stream, with the discharging bank depending on the depth of origin of the groundwater flow. This effect increases with the stream sinuosity, as can be observed by comparing Figure 5d and 5g. Furthermore, a similar, but reversed situation occurs in Figure 5c, where flow patterns are driven by the difference in hydraulic gradient in the y-direction.

In Figure 5f and 5i, the effects of stream sinuosity and a change in the flow direction at the stream are combined. The two factors have an opposing effect on results; thus, the combined effect is smoothed (compare Figure 5c, 5f, and 5i). In contrast, at meander bends pointing to the north, the effects of the meander bend and the changes in hydraulic gradient reinforce each other.

The effect of the aquifer depth on the groundwater flow to a stream on a vertical cross section perpendicular to the stream is shown in Figure 6 for the highly sinuous stream with J_{yx} of 4. In the shallow aquifer, which is 5 m deep, groundwater from the entire depth of the aquifer flows to the stream. Differently for the 40 m deep aquifer, groundwater in the top 32 m flows to the stream, while the deepest groundwater, in the lowest 8 m of the aquifer, flows horizontally beneath the stream, not being affected by the stream. When further increasing the aquifer depth up to 80 m, groundwater in the deepest 32 m of the aquifer flows horizontally downstream and is not affected by the stream. This indicates that the effect of the stream on the vertical groundwater gradient affects an area of the unconfined aquifer which increases with the aquifer depth. However, the area affected does not linearly increase with the aquifer depth and the deepest part of the aquifer is not affected by the presence of the stream.

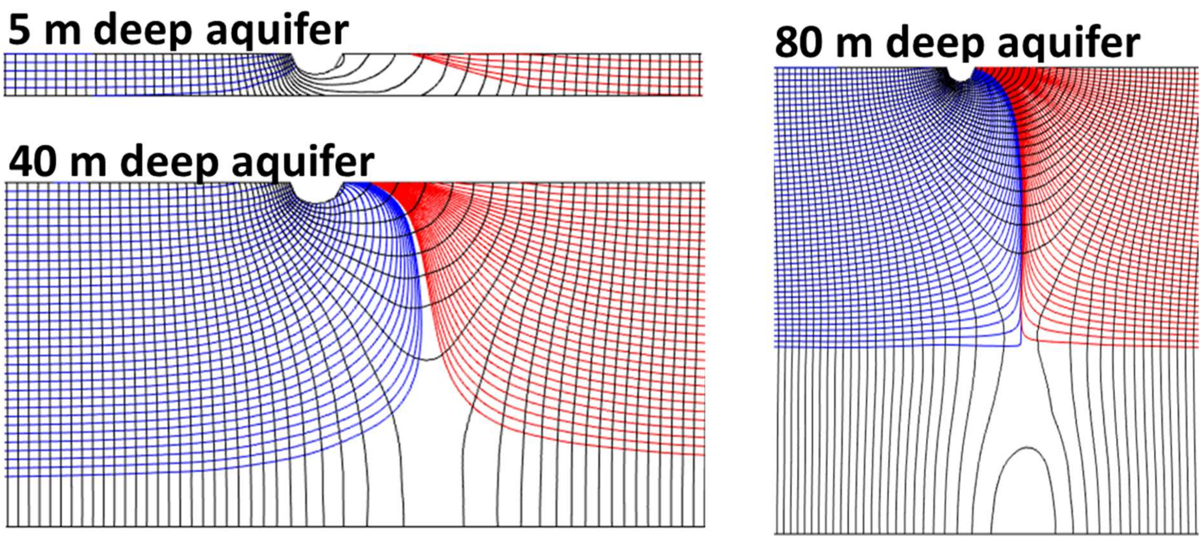

Figure 6: Effect of the aquifer depth on the groundwater paths from the northern side of the stream (red lines) and from the southern side of the stream (blue lines) at two vertical cross sections perpendicular the stream and located at the edge of a meander bend pointing north. The black lines show the equipotential lines separated by 0.1 m interval. The highly sinuous stream scenario with J_{yx} of 4 was used to implement the different aquifer depths.

The groundwater flow component in the y-direction is shown for two vertical cross sections in Figure 7: one follows the stream (Figure 7a, 7c, and 7e) and the other is centered in the middle of the model domain (Figure 7b, 7d, and 7f). The results are shown for the straight, the moderately, and the highly sinuous stream scenarios with a constant J_{yx} of 0.5. The green color indicates the absence of flow in the y-direction, the blue color indicates a negative flow, directed to the south, and the red color indicates a positive flow, directed to the north.

On the cross section following the stream, the straight stream (Figure 7a) shows that y-directional groundwater flow below the stream is zero. The results are presented only for a constant J_{yx} of 0.5 and a constant aquifer depth of 40 m, but are valid whenever the hydraulic gradient and the aquifer depths are constant. The scenario with different hydraulic gradients in the y-direction at the two sides of the stream shows groundwater flow below the stream from north to south, as shown in Figure 5c.

The moderately sinuous stream (Figure 7c) shows areas colored in blue, associated with a meander pointing toward north, and the areas colored in red, with a meander pointing south. For meanders pointing north, groundwater from the northern side of the stream flows beneath the stream in a southerly direction (the flow has a negative sign), while for meanders pointing south, groundwater from the southern side of the stream flows beneath the stream in a northerly direction (the flow has a positive sign). Between two meander extremes, an area with no flow in the y direction occurs (Figure 7c). y-directional groundwater flow under the stream is greatest for shallow depths and decreases deeper in the aquifer. The same pattern in the groundwater flows can be observed for the highly sinuous stream (Figure 7e), but is more pronounced than for the moderately sinuous stream.

The groundwater flow between the northern and southern side of the stream is further analyzed by showing the y-direction flow on a vertical cross section centered in the middle of the model domain. Curiously, this figure shows that the greatest flow of groundwater across the stream centerline occurs for the moderately sinuous stream (Figure 7d). When sinuosity increases there is less flow inside the meander bend (Figure 4), and a lower y-directional flow across the stream centerline (Figure 7e).

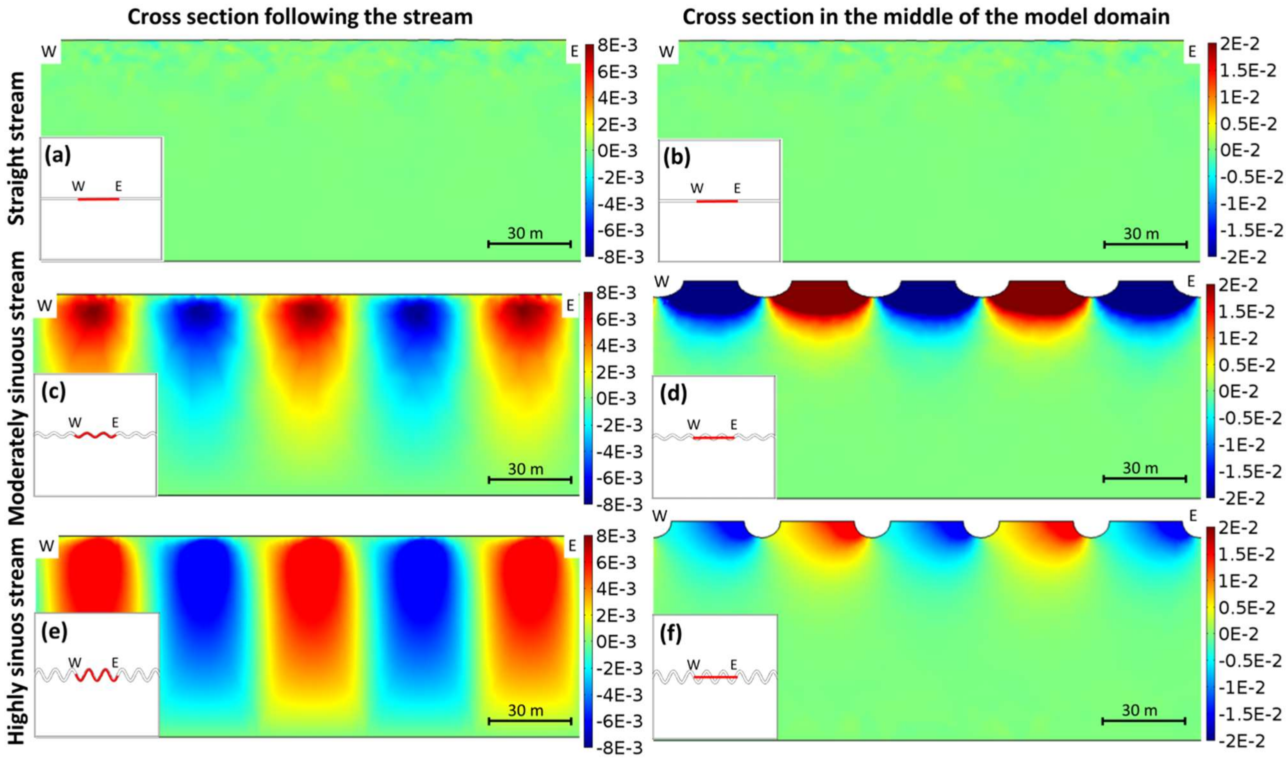

Figure 7: The color map show the groundwater flow in the y direction (qy) in m/s through a vertical cross section: one follows the stream (a, c, and e), and the other is centered in the middle of the model domain (b, d, and f). The flow has a positive value when directed to the north and a negative value when directed to the south. The results are shown for the straight, the moderately sinuous and the highly sinuous stream with J_{yx} (ratio between the hydraulic gradient in the y and x-direction) of 0.5 and an aquifer depth of 40 m. The moderately sinuous stream has sinuosity (S) of 1.14 and amplitude (α) of 5 m. The highly sinuous stream has sinuosity (S) of 1.74 and amplitude (α) of 13.5 m.

3.3 **Grindsted stream field site**

The model implemented at the Grindsted stream field site was first evaluated by comparing with the observed groundwater head and discharge to the stream. In Figure 8, the simulated groundwater head is compared to the observed head at wells located within the model domain: 114.1448 and 114.1997 (Figure 2). In well 114.1448, the model describes the variation groundwater head well, except for the period May-July 2014 when the simulated head (red line) is higher than the observed (black dots). In well 114.1997, the meandering stream model properly simulates the head until June 2014, but the head is overestimated for the remaining simulation time. The Nash-Sutcliffe efficiency coefficients (Nash and Sutcliffe, 1970) of the groundwater head simulated at the two observation wells for the entire simulation period are 0.63 and 0.68, for well 114.1448 and 114.1997 respectively. The simulated annual average groundwater discharge to the stream is 75 l/s, which matches well the annual averaged discharge estimated from the gaging stations (70 l/s). The inflow at the upgradient groundwater boundaries resembles the discharge to the stream, with small differences due to changes in storage in the domain and recharge.

The simulated groundwater discharge to the stream along the entire modeled stream stretch is shown in Figure 8 (green line). The groundwater discharge to the stream varies up to 40% during the one year simulation. The seasonal variation of the groundwater discharge to the stream is inversely related to the head in the stream and in groundwater (well 114.1448), but with a time lag due to groundwater storage. Peaks in the groundwater head close to the stream (well 114.1448) correspond to low discharges to the stream. After a groundwater peak discharge can be seen to increase, leading to an increase in stream water level. Despite this behavior, the spatial patterns of the groundwater flow to the stream in the simulations are not time varying. This is because the modeled stream is always a gaining stream, and head variations are small (up to 0.4 m over a one year simulation) compared to the aquifer thickness (80 m). We carefully note, however, that the spatial patterns of groundwater flow to the stream will probably change with time for a stream that switches between being gaining and losing conditions.

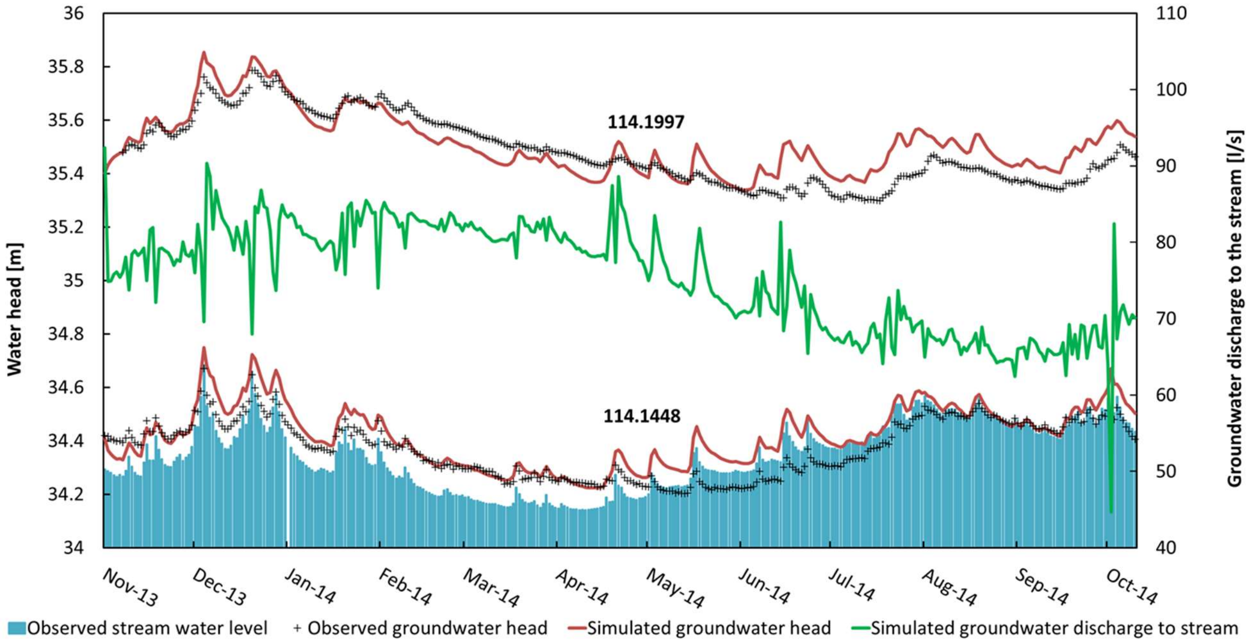

Figure 8:Model results from Grindsted stream compared to groundwater head data from well 114.1448 and 114.1997 (Figure 2). The stream water level at the closest location to well 114.1448 is indicated by the blue columns. The stream water level was calculated from the water level measurements at the Tingvejen station assuming a stream water slope, which was calculated at each day from the water level measurements at the Tingvejen and the Eg bro stations. The groundwater discharge to the stream (green line) is plotted to the secondary y-axes, which starts at 40 l/s, and is the integrated value of the discharges along the modeled stream stretch.

The horizontal groundwater flow at the upper edge of the stream-aquifer interface is shown in Figure 8 by the red arrows, whose size is proportionate to the magnitude of the flow. The groundwater discharge is not constant, but changes depending on the location along the stream. As for the sinusoidal stream geometries (Figure 4), the groundwater discharge peaks at the outside extremes of the meander bends and is smallest on the inside of the meander bends.

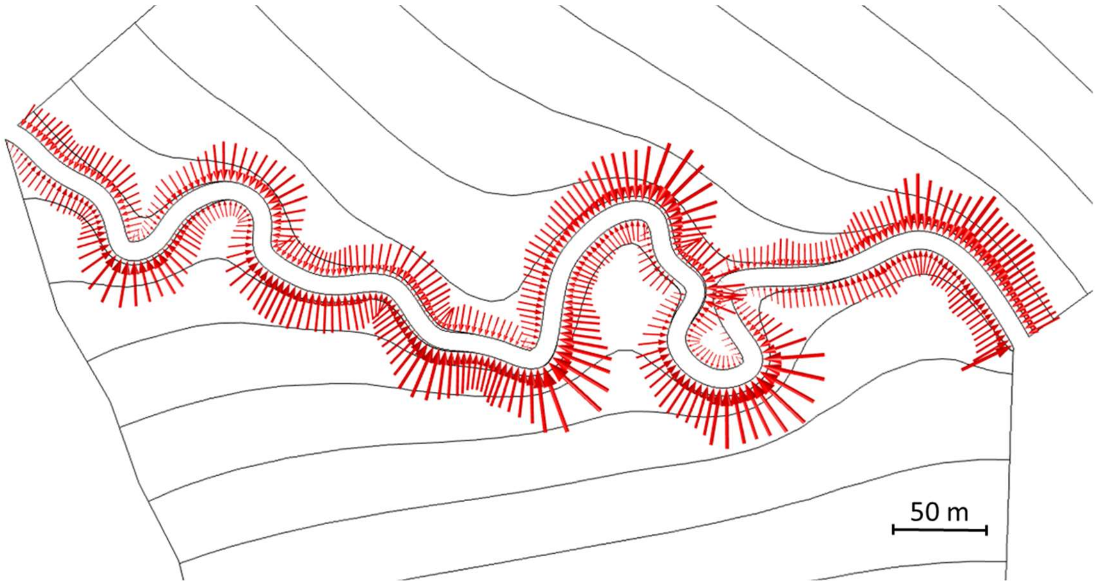

Figure 9: Horizontal groundwater flow at the upper edge of the stream-aquifer interface. The red arrows are proportional to the fluxes. The equipotential lines have a density of 0.2 m.

The groundwater flow to the stream at two vertical cross sections perpendicular to the stream is shown in Figure 10. The cross section in Figure 10a is placed at the location of a meander bend pointing to the north and the cross section in Figure 10b is placed where a meander bend is pointing to the south. In Figure 10a, the particles originating in the shallow part of the aquifer north from the stream enter the stream at the northern bank. The particles originating in the deep part of the aquifer north of the stream enter the stream on the southern bank while the particles coming from the southern side of the aquifer enter the stream on the shallow part of the southern bank. The reverse pattern is observed in Figure 9b. This is similar to the results of the moderately sinuous stream (Figure 6d and 6e) and the high sinuous stream (Figure 6g and 6h).

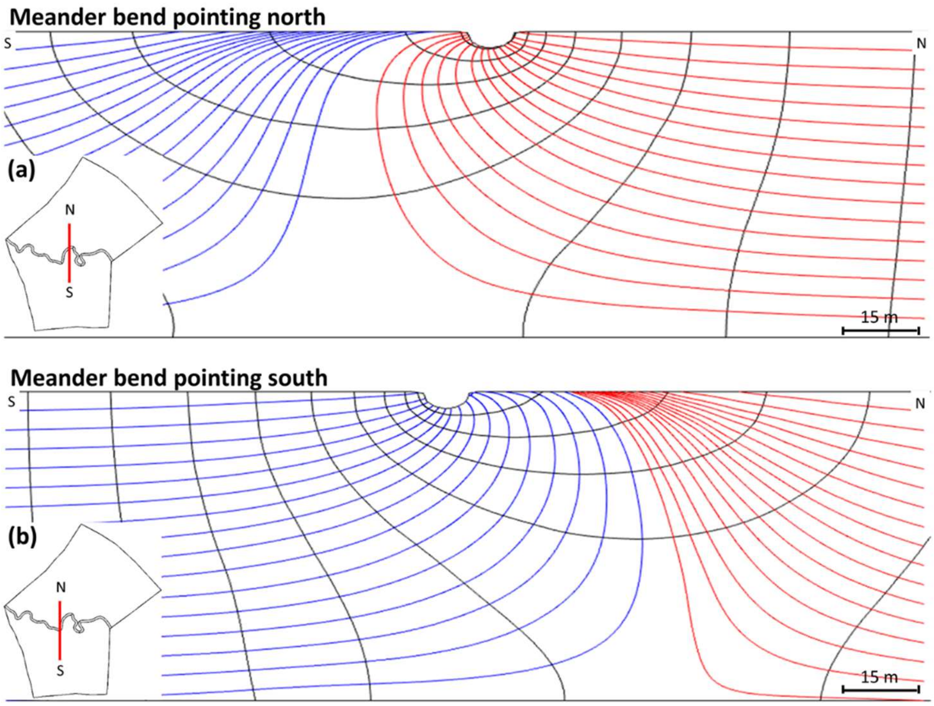

Figure 10: Groundwater paths from the northern side of the stream (red lines) and from the southern side of the stream (blue lines) at two vertical cross sections perpendicular the stream and located at the edge of a meander bend pointing north (a) and south (b). The black lines show the equipotential lines separated by 0.1 m interval.

4. Discussion

This study shows that meander bends lead to significant spatial variability in groundwater-flow to streams. The results show that most of groundwater flowing to the stream enters the stream at the outward pointing side of the meander bend, just upstream of the extremities of the meander (Figure 4 for the synthetic stream and Figure 9 for Grindsted stream). The groundwater discharge to the stream is lowest on the inside of meander bends. The amount of groundwater entering the stream is affected by the groundwater flow direction in the aquifer. In case of regional groundwater flowing in the direction of the stream, the largest groundwater flows occur on the upstream part of the outward pointing meander. For real streams, such as the Grindsted stream (Figure 9) the variations in the groundwater discharge at the stream-aquifer interface are not as regular as for the synthetic streams (Figure 4). In the synthetic streams, all meanders have the same amplitude and period and are oriented in the same way relative to the groundwater flow direction. In the Grindsted stream, the meanders have different size and are oriented differently. Thus, the spatial variability of the groundwater flow to streams is affected by the size as well as by the orientation of the meander bend.

In the field study of Weatherill et al. (2014), a high concentration of contaminants in groundwater discharge was detected at the outside of a meander bend. The results of our study, which indicate that the outward pointing side of the bends is the preferred location for groundwater discharge, help explain Weatherill et al.'s results.

The groundwater flow to the stream is observed to vary greatly with depth for both the synthetic (Figure 5, 6, and 7) and Grindsted streams (Figure 10). This confirms that groundwater flow to streams at meandering streams is three dimensional, as previously suggested by Harvey and Bencala (1993); Modica et al. (1998), and Flipo et al. (2014). The present study investigates how the vertical variability of the groundwater flow to the stream is affected by the meander bends with the discharging bank being dependent on the depth of origin of the groundwater and the stream geometry. The amount of groundwater entering the stream on the opposite bank, increases with the sinuosity (Figure 7a and 7b) and amplitude of the meanders (Figure 5). Curiously the magnitude of the flow crossing the stream center line is highest for moderately sinuous streams and decreases when increasing the sinuosity (Figure 7d and 7e). Groundwater can enter the stream on the opposite bank from its origin because of difference in hydraulic gradient in the aquifer between the two sides of the stream, as occurring when the regional groundwater flow direction is across the stream. The regional groundwater flow can either enhance or smooth the effect of the stream sinuosity, depending on the direction of the regional groundwater flow and the orientation of the meander bends.

The observation that groundwater can flow below a stream and enter the stream through the opposite bank has previously been described by Aisopou et al. (2014) and Miracapillo and Morel-

Seytoux (2014). However, the factors causing groundwater to enter the stream through the opposite bank are different in those papers than here. In Aisopou et al. (2014), the presence of a pumping well on one side of the stream creates a head gradient that forces groundwater to cross to the opposite side of the stream and enter the stream at the bank closest to the well. In Miracapillo and Morel-Seytoux (2014), the difference of the gradient between the two sides of the stream imposed by the boundary conditions, is responsible for the flow below the stream. Here we focus on the influence on stream geometry on the location of groundwater discharge to a stream.

The synthetic stream and the Grindsted stream models have been implemented using different boundary conditions. In the synthetic stream, all the lateral boundary conditions (Figure 1) are constant head and account for the head gradient in the x and y direction. In the Grindsted stream (Figure 2), the boundaries perpendicular to the stream are streamlines (no-flow boundaries) and the upstream groundwater boundaries are fixed-head. The constant head boundaries of the synthetic stream model assume no vertical groundwater gradients. As previously discussed, this is not the case close to a meandering stream. The streamline boundaries applied in the Grindsted stream model allow a vertical gradient. However, the streamline boundaries of the Grindsted model do not allow a horizontal flow across the stream lines in the aquifer. Thus along-stream groundwater flow is better modeled by constant head boundaries. Neither the no-flow nor the constant head boundary conditions perfectly describe conditions under streams. However, this paper has shown that the effect of meanders is similar for both types of groundwater boundary conditions (compare the sinusoidal examples with fixed head boundaries with the Grindsted model with the no flow boundaries), so the conclusions are robust despite boundary condition uncertainty.

The hydraulic conductivity distribution in the aquifer and in the stream bed is one of the factors, together with the stream morphology and the hydraulic gradient, known to affect the groundwater flow to streams. Recent studies by Krause et al. (2012), Brookfield and Sudicky (2013), Gomez-Velez et al. (2014), and Poulsen et al. (2015) have focused on the effect of the hydraulic conductivity distribution on the groundwater discharge to streams. Since the aim of this study is to investigate the effect of stream meanders and groundwater flow direction on the groundwater flow to streams at the reach scale, the models assume a homogenous sandy aquifer. Future studies that investigate the combined effect of stream meanders, hydraulic gradient, and hydraulic conductivity distributions would enhance the understanding on groundwater flow to streams.

5. Conclusions

A modeling study analyzing the effect of meander bends on the spatial variability of the groundwater flow in an unconfined and homogenous sandy aquifer to a gaining stream at the reach scale is presented. Results were obtained by applying the new coordinate transformation method of Boon et al. (2016) to the groundwater flow to streams problem. This problem is challenging because of the movement of the free surface upper boundary due to changes in the stream water level. The coordinate transformation method was the least computational when compared with other methods, requiring 32 times less time than the saturated-unsaturated flow and 3 times less time than moving mesh. Differences between the methods became larger when the grid is refined. Furthermore, the coordinate transformation method does not lead to the instabilities and oscillations commonly encountered with a moving mesh method. These features meant that it was possible to analyze the scenarios presented in this paper.

The results showed that presence of meander bends leads to significant spatial variability in groundwater discharge to streams. The groundwater fluxes are highest at the meander bend extremes, up to 75% of the total fluxes to a meander with a sinuosity of 1.74, and much lower on the inside of meander bends. This effect increases with the stream sinuosity. The magnitude of hydraulic gradient groundwater affects the total groundwater flux to the stream, while the direction of groundwater affects the degree of the flow to the stream. Groundwater gradients combine with the effect of stream meanders and depending on groundwater flow directions can either enhance or smooth the effect of a meander bend.

The location of the discharge of groundwater along the stream cross section is affected by the stream sinuosity, the direction of the groundwater flow, and the aquifer depth. At the meander extremes, groundwater coming from the shallow part of the aquifer enters the stream at the outward pointing bank. Groundwater coming from the deep part of the aquifer often flows beneath the stream and enters the stream at the opposite bank, at the inward side of a meander bend. The area affected by the stream on the vertical groundwater flow gradient increases with the aquifer depth, even though the deepest part of the aquifer may not be affected and groundwater flows horizontally downstream. The spatial pattern of flows to meander bends is not time dependent for a stream that is always gaining.

The field site application confirmed the finding of the synthetic study case and showed that the irregular geometry of the stream meanders affects the groundwater discharge to the stream. The difference in amplitude and orientation of meanders combines with the stream sinuosity and groundwater flow direction in determining the location and the magnitude of the water discharge to the stream. This study improved our conceptual understanding of the groundwater flow paths to meandering streams in an unconfined homogenous sandy aquifer and shows how stream meanders, combined with groundwater flow direction, affect the spatial variability of the groundwater flow to streams at the reach scale in both synthetic and field systems.

Acknowledgements

This study was supported by the research project GEOCON, Advancing GEOlogical, geophysical and CONtaminant monitoring technologies for contaminated site investigation (contract 1305-00004B). The funding for GEOCON is provided by Innovation Fund Denmark.

Additionally, this study was supported by Norwegian Research Council grant 233736. The data used in this paper can be accessed by contacting the first author Nicola Balbarini at nbal@env.dtu.dk. The authors would like to thanks Vinni Rønde, Anne Thobo Sonne and Ursula McKnight for the field data collection and their valuable assistance in the data interpretation.

References

Aisopou, A., P. J. Binning, H. Albrechtsen and P. L. Bjerg (2014), Modeling the factors impacting pesticides concentrations in groundwater wells, Groundwater, doi: 10.1111/gwat.12264.

Aisopou, A., P. L. Bjerg, A. T. Sonne, N. Balbarini, L. Rosenberg and P. J. Binning (2015), Dilution and volatilization of groundwater contaminant discharges in streams, Journal of Contaminant Hydrology, doi:10.1016/j.jconhyd.2014.11.004.

An, H., Y. Ichikawa, Y. Tachikawa, and M. Shiiba (2010), Three-dimensional finite difference saturated-unsaturated flow modeling with nonorthogonal grids using a coordinate transformation method, Water Resources Research, 46, W11521, doi:10.1029/2009WR009024.

Anibas, C., B. Verbeiren, K. Buis, J. Chorma´nski, L. De Doncker, T. Okruszko, P. Meire and O. Batelaan (2012), A hierarchical approach on groundwater-surface water interaction in wetlands along the upper Biebrza River, Poland, Hydrology and Earth System Sciences, Vol. 16, Pages 2329-2346, doi: 10.5194/hess-16-2329-2012.

Barlebo, H. C., M. C. Hill, D. Rosbjerg and K. H. Jensen (1998), Concentration Data and Dimensionality in Groundwater Models: Evaluation Using Inverse Modelling, Nordic Hydrology, 29, 149-178.

Binley, A., S. Ullah, A. L. Heathwaite, C. Heppell, P. Byrne, K. Lansdown, M. Trimmer and H. Zhang (2013), Revealing the spatial variability of water fluxes at the groundwater-surface water interface, Water Resources Research, Vol. 49, Pages, 3978-3992, doi:10.1002/wrer.20214.

Bjerg, P.L.; Rügge, K.; Pedersen, J.K.; Christensen, T.H. (1995): Distribution of redox sensitive groundwater quality parameters downgradient of a landfill (Grindsted, Denmark). Environmental Science & Technology, 29, 1387-1394.

Boano F; Camporeale C; Revelli R; Ridolfi L. (2006) Sinuosity-driven hyporheic exchange in meandering rivers, Geophys. Res. Lett., 33, L18406.

Boano, F., R. Revelli, and L. Ridolfi (2009), Quantifying the impact of groundwater discharge on the surface-subsurface exchange, Hydrological Processes, 23, 2108-2126, doi:10.1002/hyp.7278.

Boano, F., C. Camporale and R. Revelli (2010), A linear mode for the coupled surface-subsurface flow in a meandering stream, Water Resources Research, Vol. 46, W07535, doi:10.1029/2009WR008317.

Boano, F., J. W. Harvey, A. marion, A. I. Packman, R. Revelli, L. Ridolfi and A. Wörman (2014), Hyporheic flow and transport processes: Mechanisms, models, and biogeochemical implications, Review of Geophysics, Vol. 52, Pages, 603-679, doi:10.1002/2012RG000417.

Boon, W. M., N. Balbarini, P. J. Binning, and J. M. Nordbotten (2016), Efficient Water Table Evolution Discretization Using Domain Transformation, Computational Geoscience, doi:10.1007/s10596-016-9591-2.

Bresciani, E., P. Davy, and J. R. De Dreuzy (2011), A finite volume approach with local adaptation scheme for the simulation of free surface flow in porous media, Int. J. Numer. Anal. Methods Geomech., doi: 10.1002/nag.1065

Brookfield, A. E. and E. A. Sudicky (2013), Implications of hyporheic flow on temperature-based estimates of groundwater/surface water interactions, Journal of Hydrologic Engineering, 18(10), pp. 1250-1261.

Byrne, P., A. Binley, A. L. Heathwaite, S. Ullah, C. M. Heppel, K. Lansdown, H. Zhang, M. Trimmer and P. Keenan (2014), Control of river stage on the reactive chemistry of hyporheic zone, Hydrological processes, 28, 4766-4779, doi: 10.1002/hyp.9981.

Camporese, M., C. Paniconi, M. Putti and S. Orlandini (2010), Surface-subsurface flow modeling with path-based runoff routing, boundary condition-based coupling, and assimilation of multisource observation data, Water Resources Research, Vol. 46, doi:10.1029/2008WR007536.

Cardenas, M. B., J. L. Wilson and V. A. Zlotnik (2004), Impact of heterogeneity, be forms, and stream curvature on subchannel hyporheic exchange, Water Resources Research, Vol. 40, W08307, doi:10..1029/2004WR003008.

Cardenas, M. B. (2008), The effect of river bend morphology on flow and timescales of surface-groundwater exchange across pointbars, Journal of Hydrology, 362, 134-141, doi:10.1016/j.hydrol.2008.08.018.

Cardenas, M. B. (2009a), Stream-aquifer interactions and hyporheic exchange gaining and losing sinuous streams, Water Resources Research, Vol. 45, W06429, doi:10.1029/2008WR007651

Cardenas, M. B. (2009b), A model for lateral hyporheic flow based on valley slope and channel sinuosity, Water Resources Research, Vol. 45, W01501, doi:10.1029/2008WR007442.

Cey, E. E., D. L. Rudolph, G. W. Parkin and R. Aravena (1998), Quantifying groundwater discharge to a small perennial stream in southern Ontario, Canada, Journal of Hydrology, Vol. 210, Pages 21-37.

COMSOL (2013), COMSOL Multiphysics Reference Manual, Version 4.4.

Conant Jr., B., J. A. Cherry, and R. W. Gillham (2004), A PCE groundwater plume discharging to a river: influence of the streambed and near-river zone on contaminant distributions, Journal of Contaminant Hydrology, 73, 249-279, doi:10.1016/j.jconhyd.2004.04.001.

Dahl, M., B. Nilsson, J. H. Langhoff and J. C. Refsgaard (2007), Review of classification systems and new multi-scale typology of groundwater-surface water interaction, Journal of Hydrology, Vol. 344, Pages 1-16, doi:10.1016/j.jhydrol.2007.06.027.

Darbandi, M., S.O. Torabi, M. Saadat, Y. Daghighi, D. Jarrahbashi (2007), A Moving Mesh Finite-Volume Method to Solve Free-Surface Seepage Problem in Arbitrary Geometries, International Journal for Numerical and Analytical Methods in Geomechanics, Vol. 31, Pages 1609-1629.

Derx, J., A. P. Blaschke and G. Blöschl (2010), Three dimensional flow pattern at the river-aquifer interface-a case study at the Danube, Advances in Water Resources, Vol. 33, Pages 1375-1387.

Diem, S., P. Renard and M. Schirmer (2014), Assessing the effect of different river water level interpolations schemes on modeled groundwater residence times, Journal of Hydrology, Vol. 51, Pages 393-402, doi:10.1016/j.jhydrol.2013.12.049.

DMI (2015), Available from: <http://www.dmi.dk/vejr/> [20 December 2015].

Dogan A. and L. H. Motz (2005), Saturated-unsaturated 3D groundwater model. I: Development, Journal of Hydrologic Engineering, DOI: 10.1061/(ASCE)1084-0699(2005)10:6(492).

Fernando, H. J. S. (2013), Handbook of environmental fluid dynamics, CRC Press, Volume 2, Chapter 2, Pages 19-30.

Flipo, N., A. Mouhri, B. Labarthe, S. Biancamaria, A. Riviere and P. Weill (2014), Continental hydrosystem modelling: the concept of nested stream-aquifer interfaces, Hydrology and Earth System Sciences, Vol. 18, Pages 3121-3149, doi: 10.5194/hess-18-3121-2014.

Freeze, R. A. (1971), Three-Dimensional, Transient, Saturated-Unsaturated Flow in a Groundwater Basin, Water Resources Research, Vol. 7, Pages 347-366, doi:10.1029/WR007i002p00347.

Freitas, J. G., M. O. Rivett, R. S. Roche, M. Durrant, C. Walker and J. H. Tellam (2015), Heterogeneous hyporheic zone dechlorination of a TCE groundwater plume discharging to an urban river reach, Science of the Total Environment, Vol 505, Pages 236-252.

Gomez-Velez, J. D., S. Krause, and J. L. Wilson (2014), Effect of low-permeability layers on spatial patterns of hyporheic exchange and groundwater upwelling, Water Resources Research, doi:10.1002/2013WR015054.

Gomez-Velez, J.D., J.W. Harvey, M.B. Cardenas, and B. Kiel (2015), Denitrification in the Mississippi River network controlled by flow through river bedforms, Nature Geoscience, doi: 10.1038/NGEO2567.

Guay, C., M. Nastev, C. Paniconi and M. Sulis (2013), Comparison of two modeling approaches for groundwater-surface water interactions, Hydrological Processes, Vol. 27, Pages 2258-2270.

Harvey, J. W. and K. E. Bencala (1993), The Effect of Streambed Topography on Surface-Subsurface Water Exchange in Mountain Catchments, Water Resources Research, Vol. 29, No. 1, Pages 89-98.

Heron,G., Bjerg,P.L., Gravesen,P., Ludvigsen,L. & Christensen,T.H. (1998): Geology and sediment geochemistry of a landfill leachate contaminated aquifer (Grindsted, Denmark). Journal of Contaminant Hydrology, **29**, 301-317.

Karan, S., P. Engesgaard, M. C. Looms, T. Laier and J. Kazmierczak (2013), Groundwater flow and mixing in a wetland-stream system: Field study and numerical modeling, Journal of Hydrology, Vol. 488, Pages 73-83.

Keating, E. and G. Zyvoloski (2009), Saturated-unsaturated 3D groundwater model. I: Development, Ground Water, Vol. 4, Pages 569.579, doi: 10.1111/j.1745-6584.2009.00555.x.

Kinouchi, T., M. Kanda and M. Hino (1991), Numerical simulation of infiltration and solute transport in an S-shaped model basin by a boundary-fitted grid system, Journal of Hydrology, Vol. 122, Pages 373-406, doi:10.1016/0022-1694(91)90189-O.

Kjeldsen, P., P. L. Bjerg, K. Rügge, T. H. Christensen, J. K. and Pedersen, (1998), Characterization of an old municipal landfill (Grindsted, Denmark) as a groundwater pollution source: Landfill hydrology and leachate migration, Waste Management and Research, Vol 16, no. 1, pp. 14-22., doi:10.1177/0734242X9801600103.

Knupp, P. (1996), Moving mesh algorithm for 3-D regional groundwater flow with water table and seepage face, Advances in Water Resources, Vol. 19, No. 2, Pages 83-95.

Krause, S., A. Bronstert and E. Zehe (2007), Groundwater-surface water interactions in a north German lowland floodplain – Implications for the river discharge dynamics and riparian water balance, Journal of Hydrology, Vol. 347, Pages 404-417, doi:10.106/j.jhdrol.2007.09.028.

Krause, S., T. Blume, and N. J. Cassidy (2012), Investigating patterns and controls of groundwater up-welling in a lowland river by combining Fibre-optic Distributed Temperature Sensing with observations of vertical hydraulic gradients, Hydorlogy and Hearth System Sciences, 16, 1775-1792, doi:10.5194/hess-16-1775-2012.

Krause, S., F. Boano, M. O. Cutchbert, J. H. Fleckenstein and J. Lewandowski (2014), Understanding process dynamics at aquifer-surface water interfaces: An introduction to the special edition section on modeling approaches and novel experimental technologies, Water Resources Research, Vol. 50, Pages 1847-1855, doi: 10.1002/2013WR014755.

Lønborg, M.J., Engesgaard,P., Bjerg,P.L. & Rosbjerg,D. (2006): A steady state redox zone approach for modeling the transport and degradation of xenobiotic organic compounds from a landfill site. Journal of Contaminant Hydrology, 87, 191-210.

Miracapillo, C., and H. J. Morel-Seytoux (2014), Analytical solutions for stream-aquifer flow exchange under varying head asymmetry and river penetration: Comparison to numerical solutions and use in regional groundwater models, Water Resour. Res., 50, 7430–7444, doi:10.1002/2014WR015456.

Modica, E., H. T. Buxton and L. N. Plummer (1998), Evaluating the source and residence time of groundwater seepage to streams, New Jersey Coastal Plan, Water Resources Research, Vol. 34, No. 11, Pages 2797-2810.

Nalbantis, I., A. Efstratiadis, E. Rozos, M. Kopsiafti and D. Koutsoyiannis (2011), Holistic versus monometric strategies for hydrological modelling of human-modified hydrosystems, Hydrology and Earth System Sciences, Vol. 15, Pages 743-758, doi:10.5194/hess-15-743-2011.

Nash, J. E. and J. V. Sutcliffe (1970), River flow forecasting through conceptual models part I — A discussion of principles, Journal of Hydrology, 10 (3), 282–290, doi: 10.1016/0022-1694(70)90255-6

Nielsen, S. S., N. Tuxen, O. Frimodt Pedersen, P. L. Bjerg, A. T. Sonne, P. J. Binning, A. S. Fjordbøge and J. Aabling (2014), Risikovurdering af overfladevand, som er påvirket af punktkildeforurenet grundvand. Miljoeprojekter, no. 1575, Miljøstyrelsen, Miljøministeriet, København K.

Ou, G., X. Chen, A. Kilic, S. Bartelt-Hunt, Y. Li and A. Samal (2013), Environmental Modelling & Software, Vol. 50, Pages 132-143.

Poulsen, J. R., E. Sebok, C. Duque, D. Tezlaff and P. K. Engesgaard (2015), Detecting groundwater discharge dynamics from point-to-catchment scale in a lowland stream: combining hydraulic and tracer methods, Hydrology and Earth System Sciences, 19, 1871-1886, doi:10.5194/hess-19-1871-2015

Rasmussen, J. J., U. S. McKnight, A. T. Sonne, P. Wiberg-Larsen and P. L. Bjer (2015), Legacy of a chemical factory site: Contaminated groundwater impacts stream macroinvertebrates, Arch Environ Contam Toxicol, doi: 10.1007/s00244-015-0211-2.

Revelli, R., F. Boano, C. Camporale, and L. Ridolfi (2008), Intre-meander hyporheic flow in alluvial rivers, Water Resources Research, Vol. 44, doi:10.1029/2008WR007081.

Salehin, m., A. I. Packman, and M. Paradis (2004), Hyporheic exchange with heterogenous streambeds: Laboratory experiments and modeling, Water Resources Research, Vl. 40, W11504, doi:10.1029/2003WR002567.

Stonedahl, S. H., J. W. Harvey, A. Wörman, M. Salehin and A. I. Packman (2010), A multistate model for integrating hyporheic exchange from rippleds to meanders, Water Resources Management, Vol. 46, W12539, doi:10.1029/2009/WR008865.

Toth, J. (1963), A Theoretical Analysis of Groundwater Flow in Small Drainage Basins, Journal of Geophysical Research, Vol. 68, No. 16, Pages 4795-4812.

Weatherill, J., S. Krause, K. Voyce, F. Drijfhout, A. Levy and N. Cassidy (2014), Nested monitoring approaches to delineate groundwater trichloroethene discharge to a UK lowland stream at multiple spatial scales, Journal of Contaminant Hydrology, Vol. 158, Pages 38-54.

Wroblicky, G. J., M. E. Campana, H. M. Valett and C. N. Dahm (1998), Seasonal variation in surface-subsurface water exchange and lateral hyporheic area of two stream-aquifer systems, Water Resources Research, Vol. 34, No. 3, Pages 317-328